Network approach to patterns in stratocumulus clouds

Franziska Glassmeier[a,b,1] and Graham Feingold[b]

[a]National Research Council, Washington, DC 20001; and [b]Chemical Sciences Division, Earth System Research Laboratory, National Oceanic and Atmospheric Administration, Boulder, CO 80305

Stratocumulus clouds (Sc) have a significant impact on the amount of sunlight reflected back to space, with important implications for Earth's climate. Representing Sc and their radiative impact is one of the largest challenges for global climate models. Sc fields self-organize into cellular patterns and thus lend themselves to analysis and quantification in terms of natural cellular networks. Based on large-eddy simulations of Sc fields, we present a first analysis of the geometric structure and self-organization of Sc patterns from this network perspective. Our network analysis shows that the Sc pattern is scale-invariant as a consequence of entropy maximization that is known as Lewis's Law (scaling parameter: 0.16) and is largely independent of the Sc regime (cloud-free vs. cloudy cell centers). Cells are, on average, hexagonal with a neighbor number variance of about 2, and larger cells tend to be surrounded by smaller cells, as described by an Aboav–Weaire parameter of 0.9. The network structure is neither completely random nor characteristic of natural convection. Instead, it emerges from Sc-specific versions of cell division and cell merging that are shaped by cell expansion. This is shown with a heuristic model of network dynamics that incorporates our physical understanding of cloud processes.

clouds | climate | convection | self-organization | network

Clouds reflect incoming sunlight back to space and thus play an important role in modulating energy flows in the climate system. The description of shallow clouds in current global circulation models remains a challenge, however (1–3); due to computational constraints, the small scales of cloud processes cannot explicitly be resolved, and their subgrid-scale variability needs to be diagnosed (parameterized) from grid-scale mean quantities. The representation of stratocumulus (Sc) clouds, in particular, is one of the largest uncertainties for future climate projections (4, 5).

Sc clouds cover extensive parts of the subtropical oceans with an intricate tapestry of shape and structure. Satellite images reveal hexagonal cells that are reminiscent of patterns arising from Rayleigh–Bénard convection (6). Indeed, Sc fields can be considered a form of Rayleigh–Bénard convection in moist atmospheric air (7); atmospheric flow is driven by a temperature difference over the depth of the planetary boundary layer, and adiabatic cooling in upwelling regions leads to condensation and cloud formation (Fig. 1). In the absence of rain, Sc fields are arranged as approximately stationary cloudy cells separated by cloud-free rings of downwelling air (closed cells, Fig. 1*A*) (8). The formation of rain means that cloudy updraft regions develop into regions of negatively buoyant air (cold pools) as a result of sedimentation and evaporation of rain (Fig. 1*B*), (9–11). Cold pools correspond to horizontally divergent flow at the surface and are bounded by convergent rings of upwelling air that are caused by the impingement of neighboring cold pools. Cold pools thus form cloud-free cells surrounded by cloudy rings and organize into patterns of open cells that are inverse to the closed-cell case. The pattern oscillates with the life cycle of open cells, which form, grow, and spawn new cells that eventually replace the dissipating parent cells (Figs. 1*B* and 2*E*). Closed cells, with their broad updraft regions and narrow downdrafts, are driven by radiative cooling at the top of the cloudy boundary layer, while the inverse structure of open cells is driven by surface heating (12). The formation of rain is often associated with deeper, more cumuliform clouds emerging from relatively warmer sea surface temperatures. Rain can also be triggered microphysically in very clean environments. In both cases, the cold pools lead to surface-driven dynamics (Fig. 1*B*).

Although the processes governing the evolution of Sc cells have received considerable attention in recent years, the geometric structure and arrangement of cells has not been studied beyond a general recognition of an approximate hexagonality. Cellular patterns are not only typical for Rayleigh–Bénard convection but can also be observed in various other natural systems, ranging from honeycombs (13) and cell tissue (14, 15) to mud cracks (16) to polycrystals (17) and foams (18). In particular, the study of the last two examples has led to the development of a theoretical framework for the statistical analysis of cellular patterns (e.g., ref. 18) that relates to graph theory, Voronoi tessellations, and spatial networks (19). Based on this theory of natural cellular networks, we present a first characterization of the geometry of Sc cellular patterns and discuss the relationship between pattern and the underlying cloud processes. Our results could inform the development of new parameterizations of Sc in atmospheric models.

Results

Fig. 3 shows snapshots of open- and closed-cellular cloud cover from large-eddy simulations (LES) (*Materials and Methods*). We identify cells based on the horizontal divergence fields (at cloud top for cloud-top driven closed cells and at the surface for surface-driven open cells), which are more directly related to the cloud processes than, e.g., column-integrated cloud water

---

Significance

Large parts of the subtropical oceans are covered by stratocumulus (Sc) cloud decks that self-organize into honeycomb-like hexagonal patterns. These clouds cool the planet by reflecting solar radiation. Sc patterns are controlled by processes from the micrometer to the kilometer scale. Climate models cannot resolve these length scales, such that Sc clouds are a large uncertainty for climate projections. Inspired by similar patterns in biology and physics, we analyze Sc patterns as dynamic cellular networks. This perspective enables us to translate detailed knowledge of cloud processes into a simple network model. Our model offers a fundamental explanation of the structure and arrangement of Sc clouds and may contribute to improving their representation in climate models.

Fig. 1. Conceptual sketch of processes leading to Sc clouds. (*A*) The extensive cloud cover of closed-cell Sc causes significant radiative cooling at the top of the cloud layer (blue shading) that sustains a top-driven circulation of narrow downdrafts (blue arrows) and broad updrafts (red arrows). In the upper section of the updrafts, atmospheric air is sufficiently cooled by adiabatic expansion for condensation of water vapor to form clouds. From the top view, cloudy cells of warmer rising air (red shading and ⊙ symbol) are surrounded by rings of colder, sinking air (blue line). (*B*) Strong narrow updrafts (red arrows) result in clouds deep enough to develop into shafts of rain (blue stippling). Sedimentation of rain and, more so, its evaporation in the subcloud layer (thinning of stippling) cause broad downdrafts, or cold pools, (blue arrows). At the surface, the outflows from neighboring cold pools force new updrafts (red arrows). A sea surface warmer than the adjacent air (red shading) can additionally trigger and support strong updrafts. The top view illustrates that the strongest updrafts (red symbol ⊙) emerge at the intersection of the outflow boundaries (red lines) of three, rather than two, cold pools (blue symbol ⊗). The oscillatory temporal evolution from clouds to cold pools to new clouds is depicted in Fig. 2*E*.

(cloud water path). A Voronoi tessellation based on cell centers is applied to define a planar, spatial network of cloud cells as illustrated in Fig. 3, where nodes correspond to cells and links connect nearest neighbors (e.g., ref. 19, section 2.1).

Cloud Network Characteristics. The cloud field rearranges with time such that the derived network is time-dependent. Similar to epidermal tissue but in contrast to the slow coarsening of foams (20), it evolves approximately as a dynamic steady state where the average number of cells, i.e., the average cell size, is constrained by the aspect ratio of atmospheric Rayleigh–Bénard cells (Fig. S1). For our statistical analysis, we consider network data from all steady-state time steps as samples.

The average area of n-sided cells, $\langle A_n \rangle$, scales with the average cell area $\langle A \rangle$ as well as with the number of sides n (Fig. S2 *A* and *B*),

$$\frac{\langle A_n \rangle}{\langle A \rangle} = 1 - \lambda \cdot (6 - n). \quad [1]$$

This relationship is known as Lewis's Law (15, 21, 22), and the parameter λ is characteristic of the specific system under study (Table 1). As an important consequence, the cell arrangement as described by the network characteristics is independent of the average cell size, which corresponds to the typical length scale of the system. Pattern in Sc can be considered scale-invariant in this sense.

Due to Lewis's Law, the distribution of relative cell sizes $\langle A_n \rangle / \langle A \rangle$ corresponds to the distribution of nearest neighbors, i.e., to the degree distribution of the network. The distributions in Fig. 4 *A* and *B* show that the Sc patterns for closed as well as open cells are a mixture of pentagons, hexagons, and heptagons, with a few four- and eight-sided cells. The distributions are peaked at six (Fig. 4 *A* and *B*) such that cloud cells are, on average, hexagonal. According to Euler's Formula from graph theory in two dimensions, this is a consequence of the triple junctions featured by cloud and Voronoi cells (Fig. 3 and ref. 21). For irregular Voronoi tessellations, nontriple junctions are very improbable. In evolving systems, quadruple junctions break up into two triple junctions as a result of random fluctuations of cell walls. In physical systems with surface tension, the breakup is not random, but is driven by the local minimization of the interface length, which is reduced for two triple compared with a quadruple junction. Unlike, e.g., foams, cloud cells do not feature a surface tension. Nevertheless, the dynamic pressure at the boundary of expanding cold pools acts equivalently to the Laplace pressure resulting from surface tension. In both cases, the temporal evo-

lution strives to decrease local curvature, corresponding to the local minimization of the interface. Given the widespread occurrence of approximately hexagonal structures, the variance of the neighbor number distribution, σ^2, rather than its mean, is used for characterization of the network (Table 1).
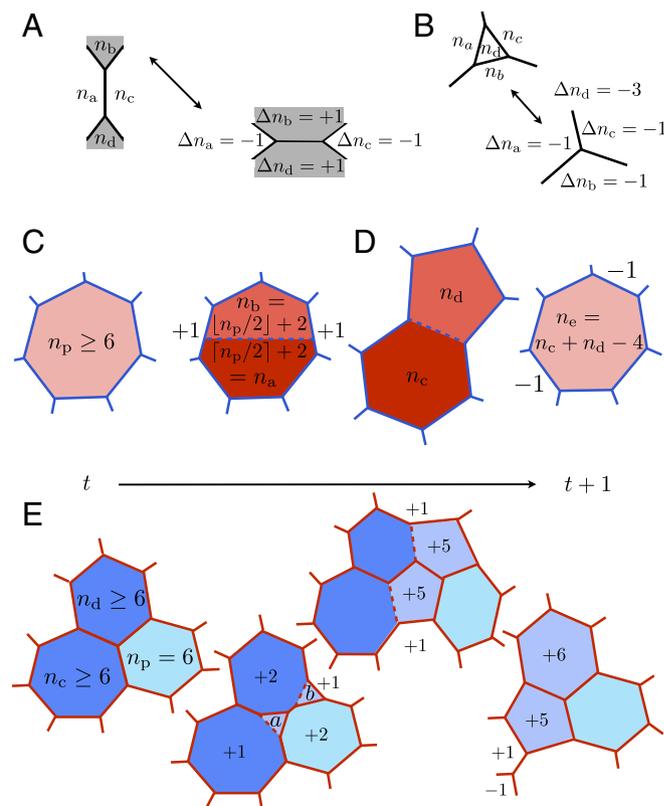
Fig. 2. Network dynamics. Transformations on triple junction networks can be decomposed into (*A*) edge flips and (*B*) the appearance or disappearance of triangular cells. They correspond to changes Δn in edge number n. Closed-cell Sc dynamics can be conceptually modeled as (*C*) cell division and (*D*) cell merging. (*E*) Open-cell dynamics feature spatially collocated appearance of new cells, cell growth by edge flips, and cell disappearance (example realization shown). Colors correspond to the top views in Fig. 1.

Fig. 3. Illustration of cloud-cell networks for (*A*) closed-cell and (*B*) open-cell Sc. The figure shows cloud water path [white for values larger than >0.07 mm (*A*) or >0.1 mm (*B*); gray otherwise], horizontal divergence field [(*A*) at cloud top, pink contour at -0.009 s^{-1}; (*B*) at the surface, contour at -0.003 s^{-1}] and Voronoi tessellation (cell centers and boundaries in green) for typical snapshots [simulation time (*A*) 450 min and (*B*) 825 min]. Exemplary triple junctions are highlighted by Y-shaped lines.

The average number of sides featured by the cells surrounding an n-sided cell, $\langle N_n \rangle$, characterizes the arrangement of cells. We find that the Sc network fulfills the Aboav–Weaire Law (17, 21, 23) (Fig. S2 *C* and *D*),

$$\langle N_n \rangle = (6 - a) + \frac{6a + \sigma^2}{n}. \qquad [2]$$

Here, the number N_n decreases with n if $a/\sigma^2 + 1/6 > 0$, which corresponds to larger cells being surrounded by smaller cells and vice versa. Otherwise, large and small cells cluster separately. For Sc (Table 1), large (many-sided) cloud cells are surrounded by smaller (few-sided) ones. This is consistent with the continuously renewing dynamics of Sc fields, in which growing new (small) cells replace older (larger) cells, as will be discussed in more detail in *Heuristic Model for Cloud Organization*.

It is interesting to note that the Lewis and Aboav–Weaire laws are related to the system entropy. A violation of these laws would indicate that the system is prevented from further maximizing its entropy by system-specific constraints [maximum entropy formalism (21, 24, 25)]. Accordingly, Sc cell networks are as random as allowed by general geometrical, topological, and statistical constraints, and there are no external factors that would increase the order of the system.

Entropy maximization results in a certain relationship between cell size and neighbor number (Lewis's Law) and certain neighbor correlations (Aboav–Weaire Law) but does not prescribe the parameters σ^2, λ, and a. Their values and the corresponding network structure thus encode information about the system-specific processes shaping the network. Table 1 summarizes the characteristics of open- and closed-cell Sc networks and shows that they share very similar parameter values despite the distinctly different cloud processes underlying the two regimes. Only the variance of the neighbor number distribution σ^2 tends to be slightly larger for the open-cell case. The Sc network parameters are, however, distinctly different from Voronoi networks derived from randomly placed points, as well as being different from observational results for solar granulation (26) and experimental Bénard–Marangoni convection (27). This indicates that Sc convection is shaped neither by randomness nor by rules generic to natural convection. Sc patterns instead emerge from processes common to open and closed cells, as explored in the following.

The characteristics of the Sc networks emerge as a dynamic steady state from the evolution of specific network dynamics

that continuously rearranges cloud cells. For a 2D natural cellular network with triple junctions, there are two elemental transformations that preserve triple junctions, and into which more complicated transformations can be decomposed (28): edge flips (Fig. 2*A*) and the appearance or disappearance of a triangular cell (Fig. 2*B*). Edge flips redistribute the number of edges between neighboring cells. In combination with Lewis's Law, they thus correspond to the growth of cells at the expense of neighboring cells. Appearance or disappearance changes the total number of cells in a network.

The effect of a network transformation leaves a topological scar (e.g., ref. 29), i.e., it changes the neighbor numbers of collocated cells in a distinct way. To allow for a statistical evaluation,

Table 1. Comparison of network properties based on LES, examples of natural convection from the literature, and heuristic network models

Source	$\langle n \rangle$	σ^2	λ	a	$\frac{a}{\sigma^2} + \frac{1}{6}$
LES					
Closed cells	6	1.8	0.16	0.93	0.7
Open cells	6	2.4	0.17	0.87	0.5
Literature					
Random Voronoi network	6	1.78	0.25	0.75	0.59
Solar granulation	6	1.78	0.25	>0.75	>0.59
Bénard–Marangoni convection	6	0.2–0.8	0.23	1.4	1.9–7.2
Network models					
Random flips	6	10.6	–	−0.79	0.1
Biased flips	6	1.2	–	0.77	0.8
Closed cells	6	1.3	–	0.35	0.4
Open cells	6	1.4	–	−0.20	+0.0

Listed are the average number of neighbors *n*, the variance of the neighbor number distribution σ^2, the Lewis parameter λ (not applicable for the purely topological network models), and the Aboav parameter *a*. Positive values in the last row indicate that larger cells are surrounded by smaller ones (see *Cloud Network Characteristics*). LES-derived and model values are rounded to the accuracy indicated by LES sensitivity tests to the evaluation parameters (*Materials and Methods*). Literature values for the random Voronoi network are based on refs. 33–36, and values for Bénard–Marangoni convection are based on ref. 27. The values for solar granulation are inferred from ref. 26, who describe solar granulation as a random Voronoi network with slightly increased order in cell arrangement. For random flips, our model is in accordance with analytical derivations of ref. 37.

Fig. 4. (*A–D*) Neighbor number distributions, which are equivalent to the size and degree distribution (see *Cloud Network Characteristics*), with variance σ^2 and (*E–H*) topological scar (see *Cloud Network Characteristics*) for the LES-derived (*A* and *E*) closed- and (*B* and *F*) open-cellular networks and for the networks resulting from the (*C* and *G*) closed-cell and (*D* and *H*) open-cell heuristic network model.

we visualize topological scars as a pattern of pairs $(\Delta n_1, \Delta n_2)$ in a diagram accounting for the changes in the number of neighbors $\Delta n_1 < \Delta n_2$ of two neighboring cells. As illustrated in Fig. 2*A*, flips are characterized by $(\Delta n_1, \Delta n_2) \in \{(-1,0), (-1,+1), (0,+1), (+1,+1)\}$. The appearance of a cell corresponds to $(\Delta n_1, \Delta n_2) \in \{(0,+1), (+1,+1), (+1,+3)\}$, and the disappearance corresponds to $(\Delta n_1, \Delta n_2) \in \{(-3,-1), (-1,-1), (-1,0)\}$. Fig. 4 *E* and *F* shows the topological scars resulting from the temporal evolution of the LES-derived cloud networks. In accordance with the very similar network characteristics in Table 1, closed- and open-cell networks feature very similar topological scars. This indicates that the open- and closed-cell networks are governed by comparable network dynamics. Both scars bear the imprint of flips (center of the plots) along with the appearance and disappearance of six-sided cells [peaks at $(\Delta n_1, \Delta n_2) = (0, \pm 6)$] and the simultaneous appearance or disappearance of two neighboring six-sided cells [$(\Delta n_1, \Delta n_2) = (\pm 6, \pm 6)$]. The appearance of six-sided cells combines the appearance of a three-sided cell with three consecutive edge flips that increase the new cell's neighbor number. This means that we do not fully resolve elemental transformations in our analysis. The simultaneous appearance of two cells indicates a spatial asymmetry of the spawning process such that new cells emerge at neighboring vertices rather than in a triangular arrangement that would promote a perfectly hexagonal grid.

Heuristic Model for Cloud Organization. Combining elemental transformations, we propose network dynamics T_{closed} for closed-cellular (Fig. 2 *C* and *D*) and T_{open} for open-cellular (Fig. 2*E*) networks that encapsulate our physical understanding of the corresponding cloud processes (also see *Supporting Information*): For the oscillatory dynamics of the open-cell case, a parent cell with $n_p = 6$ neighbors can potentially spawn new cells at all of its vertices. The development of a new cell, however, requires space for expansion. This is given in the neighborhood of older and larger cells with $n_{c/d} \geq 6$, which are weakened as a result of dissipating rain. We assume that new cells quickly expand at the expense of these cells until both cells have similar sizes with $n_{a/b/c/d} \geq 5$. To conserve the overall number of cells, the time step is finalized by the disappearance of cells c and d.

The quasi-stationary closed-cell dynamics is less structured, and its evolution consists of spatially separated pairs of cell division (Fig. 2*C*) of cells with $n_p \geq 6$ neighbors and cell merging

(Fig. 2*D*). Cell division and merging can be decomposed into the appearance, or disappearance, of a new cell and edge flips (Fig. S3 *A–I*). When not resolving the intermediate steps including triangular cells, the open-cell dynamics can thus be considered a double cell division followed by a double cell merging at the same location (see *Supporting Information*). In this sense, the dynamics governing open and closed cells are equivalent, which explains the very similar neighbor number distributions and topological scars. Our analysis does not fully resolve the intermediate steps because it is difficult to separate fluctuations that are not part of the organized convective motion from newly emerging cells. The intermediate occurrence of these cells is, however, reflected in the slightly larger variance σ^2 of the open-cell neighbor number distribution (Table 1).

As illustrated in Fig. 4 *E* and *F*, edge flips occur much more frequently than cell appearance and disappearance events. The way of choosing edges for flips can thus strongly influence the network properties: Table 1 and Fig. S4*A* illustrate the network properties resulting from iteratively applying flips F_{rand} to randomly chosen edges of an initial network (see *Supporting Information*). The result is a very broad size distribution where few-sided cells are more populated than many-sided cells, because the latter are more likely to be randomly selected for edge flipping. This scenario of edge flipping is not congruent with cloud field dynamics, where edge flips are driven by the expansion of small cells (30). We account for this bias by selecting those edges of a given cell for which $n_b + n_d$ in Fig. 2*A* is smallest. The network resulting from edge flips F_{bias} biased in this manner is peaked at six (Fig. S4*B*). The specific bias of flips can be considered as an adjustable "parameter" of the network model that is needed to capture the details of the physical system that are lost when interpreting it as a network. This has been illustrated for foam ripening, where experimental results of $a \approx 1.2$ (31) are reproduced when explicitly taking surface tension into account for determining edge flips (32), but not for random flips (24). The identical bias for open and closed cells contributes to their equivalent network evolution. Examples of natural convection with differing network structure likely feature other biases.

Based on the rules T_{closed} and T_{open}, we can model the evolution of a cloud network by iteratively applying them at random locations, starting from a suitable initial network (see *Supporting Information*). To mimic the competition of cells for space independent of cell division or merging events, we add two

edge flips F_{bias} at random locations for each application of T_{closed} or T_{open}. Apart from the initial condition, whose influence vanishes as the network approaches the steady state that is consistent with the iteratively applied network dynamics, this network model is independent of the LES simulations. Fig. 4 *C*, *D*, *G*, and *H* illustrates the resulting neighbor number distributions and topological scars. They are, on the one hand, very similar for the heuristic models of open and closed cells, which confirms that both are equivalent. On the other hand, they are in reasonable agreement with the LES-derived results, where the two additional edge flips ensure an appropriate weighting of flips compared with cell appearance and disappearance. Network parameter values are listed in Table 1 and show qualitative agreement with $\sigma^2 > 1$ and values of a such that larger cells are surrounded by smaller ones. The network model can thus qualitatively explain the emergence of the network characteristics derived from LES.

Discussion and Conclusion

We have presented a first analysis of the geometric structure and organization of cellular patterns in Sc cloud fields. We demonstrate that these patterns can be described as natural cellular networks (Fig. 3). Our network analysis shows that different Sc fields share a common structure that is independent of the details of boundary layer and cloud processes: As a consequence of entropy maximization, the size of an individual Sc cell scales with the average cell size in the Sc field and with its number of neighboring cells (Lewis's Law, Eq. **1**). This scale independence means that the pattern in Sc does not encode information about determinants of Sc evolution like boundary layer depth, sea surface temperature, aerosol concentration, or rain rate. This complexity is instead encapsulated in the average cell size.

The macroscopic Sc pattern emerges from local transformation rules. By proposing a heuristic model of network dynamics (Fig. 2), we explain that the characteristics of cloud networks follow from the random interplay of expansion and weakening of convective outflows: Cell growth, corresponding to the expansion of convective outflows and represented by edge flips with a characteristic bias, is the most frequently occurring transformation (Fig. 4 *E* and *F*). The local dynamics of convective outflows follows the laws of hydrodynamics and is thus largely independent of the scale and regime (open vs. closed) of the convection. In addition, the network transformations mimicking the differing underlying cloud processes that create closed as opposed to open cells (Fig. 1) are equivalent and are both given by forms of cell division and cell merging (Fig. 2). As a consequence, Sc cell arrangement is the same for open and closed cells.

The details of network transformation rules determine the numerical parameters that characterize the structure of the Sc cell network (Table 1): Sc cells are, on average, hexagonal (Fig. 4 *A* and *B*), because the competition of convective outflows for space results in triple junctions of cell walls (Fig. 3). For triple junctions in two dimensions, hexagonality is a mathematical necessity (Euler's formula). Nonhexagonal cells are arranged such that larger cells are surrounded by smaller ones. Although qualitatively in agreement, the parameter values for Sc do not seem universal to natural convection, as they differ from those of Bénard–Marangoni convection (27) and solar granulation (26). Future studies based on heuristic network models could reveal the system specifics behind these differences.

The heuristic model of network dynamics extends the current process understanding, especially of open cell Sc. It illustrates that the spawning of new cells in open-cell Sc happens at neighboring vertices, located next to a common area of decaying cells that allows for the expansion of newly formed cells. Our analysis thus confirms (38) that the arrangement of rainy patches is crucial to open-cell dynamics and provides guidance on the details of the required arrangement. From a systemic point of view, the network analysis reveals that the self-organization of the open-cell pattern does not require system-wide synchronization in the sense of an intimate timing of the oscillatory evolution of distant clouds as investigated by ref. 39. Instead, the open-cell pattern is obtained from local random transformations that are constrained by topology and geometry. Along the same lines, because the nodes of the Sc network have a narrow degree distribution (Fig. 4 *A–D*), there are no cells that take on the role of central hubs as speculated by ref. 40. Only on the local level is it the parent nodes that drive the network rearrangement.

In combination with information about the average cell size and the cell regime (closed vs. open), our results describe the spatial structure in Sc-topped boundary layers that is required to explicitly parameterize subgrid-scale variability in low-resolution atmospheric models. Along the lines of ref. 41, both average cell size and regime can be related to the slow manifold of Sc evolution. Slowly evolving variables (timescale of days), notably the boundary layer height, provide boundary conditions for processes on faster timescales (timescale of hours). The size of Sc cells is known to scale with the depth of the boundary layer based on a fairly well-constrained aspect ratio (cell diameter:boundary layer depth) between 1:30 and 1:40 (42). The average cell size can thus be considered a slowly evolving variable. The cell regime is also related to the boundary layer depth in that open cells become more probable than closed cells with increasing boundary layer height (Fig. 1). As a second dimension, the dynamic evolution of the background aerosol concentration can control the slow evolution of the cell regime (43, 44). The proposed heuristic modeling of network dynamics describes the evolution on the fast manifold. It is universal and independent of the evolution of the slow variables that emerges from the complex interplay of boundary layer processes. Thus, the disentangling of process complexity and cloud pattern provided by our network analysis presents a kind of simplification usually not achieved for atmospheric processes and suggests that new approaches from dynamical systems theory have great potential for atmospheric science in general and clouds in particular.

Materials and Methods

We perform LES with the System for Atmospheric Modeling (45) with the same setup as used by ref. 46 (zero horizontal winds in the initial state). The Sc case is based on observed initial and boundary conditions [Dynamics and Chemistry of Marine Sc Field Study II, Research Flight 02 (47)], which have a tendency to transition from the closed- to the open-cell regime when drop concentration is sufficiently low. Following ref. 46, we obtain an open-cell simulation by reducing the number of cloud droplets from 90 mg^{-1} to 15 mg^{-1} using the time series prescribed in ref. 46. Details of the LES setup are given in Table S1. The LES model output is available from the authors upon request. To identify cells, cell walls are completed and broadened by applying a minimum filter to the divergence field, which replaces the original values in the footprint region of the filter by the region's minimum value. Cells are then defined as contiguous regions with divergence larger than a threshold value of 0.009 s^{-1} for closed cells, and 0.003 s^{-1} for open cells. For closed and open cells, only features larger than 0.3675 km^2, or 2 km^2, respectively, are considered cells. The results were found to be robust when varying threshold and feature size up to a factor of 2. We find the centers of these cells by calculating the center of mass of the divergence field within each cell. Cells are tracked in time by assuming that the center of a cell does not move more than half the cell's extension in both horizontal directions from one time step to the next. A heuristic description of the algorithms for the network model can be found in *Supporting Information*. The full python code is available online (https://github.com/fglassmeier/cellnet). Representative results obtained with a single random seed are shown.

1. Schneider T, et al. (2017) Climate goals and computing the future of clouds. *Nat Clim Change* 7:3–5.
2. Sherwood SC, Bony S, Dufresne JL (2014) Spread in model climate sensitivity traced to atmospheric convective mixing. *Nature* 505:37–42.
3. Bony S, Dufresne JL (2005) Marine boundary layer clouds at the heart of tropical cloud feedback uncertainties in climate models. *Geophys Res Lett* 32:L20806.
4. Boucher O, et al. (2013) *Clouds and Aerosols in Climate Change 2013: The Physical Science Basis. Contribution of Working Group I to IPCC AR5*, eds Stocker TF, et al. (Cambridge Univ Press, Cambridge, UK).
5. Myhre G, et al. (2013) Anthropogenic and natural radiative forcing. *Climate Change 2013: The Physical Science Basis. Contribution of Working Group I to IPCC AR5*, eds Stocker TF, et al. (Cambridge Univ Press, Cambridge, UK), pp 659–740.
6. Getling AV, Brausch O (2003) Cellular flow patterns and their evolutionary scenarios in three-dimensional Rayleigh-Bénard convection. *Phys Rev E* 67:046313.
7. Krishnamurti R (1975) On cellular cloud patterns. Part 1: Mathematical model. *J Atmos Sci* 32:1353–1363.
8. Koren I, Feingold G (2013) Adaptive behavior of marine cellular clouds. *Sci Rep* 3:2507.
9. Xue H, Feingold G, Stevens B (2008) Aerosol effects on clouds, precipitation, and the organization of shallow cumulus convection. *J Atmos Sci* 65:392–406.
10. Savic-Jovcic V, Stevens B (2008) The structure and mesoscale organization of precipitating stratocumulus. *J Atmos Sci* 65:1587–1605.
11. Sharon TM, et al. (2006) Aerosol and cloud microphysical characteristics of rifts and gradients in maritime stratocumulus clouds. *J Atmos Sci* 63:983–997.
12. Helfand HM, Kalnay E (1983) A model to determine open or closed cellular convection. *J Atmos Sci* 40:631–650.
13. Nazzi F (2016) The hexagonal shape of the honeycomb cells depends on the construction behavior of bees. *Sci Rep* 6:28341.
14. Dubertret B, Rivier N (2000) Geometrical models of the renewal of the epidermis. *Life Sci* 323:49–56.
15. Lewis FT (1928) The correlation between cell division and the shapes and sizes of prismatic cells in the epidermis of cucumis. *Anat Rec* 38:341–376.
16. Goehring L, Morris SW (2014) Cracking mud, freezing dirt, and breaking rocks. *Phys Today* 67:39–44.
17. Aboav DA (1970) The arrangement of grains in a polycrystal. *Metallography* 3:383–390.
18. Sadoc JF, Rivier N, eds (1999) *Foams and Emulsions*, Nato Science Series E (Springer, New York).
19. Barthélemy M (2011) Spatial networks. *Phys Rep* 499:1–101.
20. Dubertret B, Aste T, Ohlenbusch HM, Rivier N (1998) Two-dimensional froths and the dynamics of biological tissues. *Phys Rev E* 58:6368–6378.
21. Rivier N (1999) Statistical thermodynamics of foam. *Foams and Emulsions*, Nato Science Series E (Springer, New York), pp 105–126.
22. Lewis FT (1931) A comparison between the mosaic of polygons in a film of artificial emulsion and the pattern of simple epithelium in surface view. *Anat Rec* 50:235–265.
23. Weaire D (1974) Some remarks on the arrangement of grains in a polycrystal. *Metallography* 7:157–160.
24. Peshkin MA, Strandburg KJ, Rivier N (1991) Entropic predictions for cellular networks. *Phys Rev Lett* 67:1803–1806.
25. Rivier N, Lissowski A (1982) On the correlation between sizes and shapes of cells in epithelias mosaics. *J Phys A: Math Gen* 15:L143–L148.
26. Schrijver CJ, Hagenaar HJ, Title AM (1997) On the patterns of the solar granulation and supergranulation. *Astrophys J* 475:328–337.
27. Cerisier P, Rahal S, Rivier N (1996) Topological correlations in Bénard-Marangoni convective structures. *Phys Rev E* 54:5086–5094.
28. Weaire D, Rivier N (1984) Soap, cells and statistics—Random patterns in two dimensions. *Contemp Phys* 25:59–99.
29. Miri M, Rivier N (2006) Universality in two-dimensional cellular structures evolving by cell division and disappearance. *Phys Rev E* 73:031101.
30. Kazil J, Yamaguchi T, Feingold G (2017) Mesoscale organization, entrainment, and the properties of a closed-cell stratocumulus cloud. *J Adv Model Earth Syst*, 10.1002/2017MS001072.
31. Aboav DA (1980) The arrangement of cells in a net. *Metallography* 13:43–58.
32. Sprague AP, Patterson BR, Grandhi S (2010) Topological characteristics of two-dimensional grain growth-simulation and analysis. *Metall Mater Trans A* 41:592–602.
33. Hilhorst HJ (2006) Planar Voronoi cells: The violation of Aboav's law explained. *J Phys A: Math Gen* 39:7227–7243.
34. Hilhorst HJ (2005) Asymptotic statistics of the n-sided planar Poisson–Voronoi cell: 1. Exact results. *J Stat Mech Theor Exp* 2005:P09005.
35. Tanemura M (2003) Statistical distributions of Poisson Voronoi cells in two and three dimension. *Forma* 18:221–247.
36. Boots BN (1982) The arrangement of cells in "random" networks. *Metallography* 15:53–62.
37. Godreche C, Kostov I, Yukutieli I (1992) Topological correlations in cellular structures and planar graph theory. *Phys Rev Lett* 69:2674–2677.
38. Yamaguchi T, Feingold G (2014) On the relationship between open cellular convective cloud patterns and the spatial distribution of precipitation. *Atmos Chem Phys* 15:1237–1251.
39. Feingold G, Koren I (2013) A model of coupled oscillators applied to the aerosol-cloud-precipitation system. *Nonlin Process Geophys* 20:1011–1021.
40. Feingold G, Koren I, Wang H, Xue H, Brewer WA (2010) Precipitation-generated oscillations in open cellular cloud fields. *Nature* 466:849–852.
41. Bretherton CS, Uchida J, Blossey TN (2010) Slow manifolds and multiple eqilibria in stratocumulus-capped boundary layers. *J Adv Model Earth Syst* 2:14.
42. Wood R, Hartmann DL (2006) Spatial variability of liquid water path in marine low cloud: The importance of mesoscale cellular convection. *J Clim* 19:1748–1764.
43. Berner AH, Bretherton CS, Wood R, Muhlbauer A (2013) Marine boundary layer cloud regimes and POC formation in a CRM coupled to a bulk aerosol scheme. *Atmos Chem Phys* 13:12549–12572.
44. Kazil J, et al. (2011) Modeling chemical and aerosol processes in the transition from closed to open cells during VOCALS-REx. *Atmos Chem Phys* 11:7491–7514.
45. Khairoutdinov MF, Randall DA (2003) Cloud resolving modeling of the ARM summer 1997 IOP: Model formulation, results, uncertainties, and sensitivities. *J Atmos Sci* 60:607–625.
46. Feingold G, Koren I, Yamaguchi T, Kazil J (2015) On the reversibility of transitions between closed and open cellular convection. *Atmos Chem Phys* 15:7351–7367.
47. Ackerman AS, et al. (2009) Large-eddy simulations of a drizzling, stratocumulus-topped marine boundary layer. *Mon Weather Rev* 137:1083–1110.